Near-degeneracy of extended $s + d_{x^2-y^2}$ and d_{xy} order parameters in quasi-two-dimensional organic superconductors

Daniel Guterding,* Michaela Altmeyer, Harald O. Jeschke, and Roser Valentí
Institut für Theoretische Physik, Goethe-Universität Frankfurt, Max-von-Laue-Straße 1, 60438 Frankfurt am Main, Germany
(Received 23 May 2016; published 19 July 2016)

The symmetry of the superconducting order parameter in quasi-two-dimensional bis-ethylenedithio-tetrathiafulvalene (BEDT-TTF) organic superconductors is a subject of ongoing debate. We report *ab initio* density-functional-theory calculations for a number of organic superconductors containing κ-type layers. Using projective Wannier functions, we derive the parameters of a common low-energy Hamiltonian based on individual BEDT-TTF molecular orbitals. In a random-phase approximation spin-fluctuation approach, we investigate the evolution of the superconducting pairing symmetry within this model, and we point out a phase transition between extended $s + d_{x^2-y^2}$ and d_{xy} symmetry. We discuss the origin of the mixed order parameter and the relation between the realistic molecule description and the widely used dimer approximation. Based on our *ab initio* calculations, we position the investigated materials in the obtained molecule model phase diagram, and we simulate scanning tunneling spectroscopy experiments for selected cases. Our calculations show that many κ-type materials lie close to the phase-transition line between the two pairing symmetry types found in our calculation, possibly explaining the multitude of contradictory experiments in this field.

DOI: 10.1103/PhysRevB.94.024515

I. INTRODUCTION

Quasi-two-dimensional organic charge-transfer salts of bis-ethylenedithio-tetrathiafulvalene molecules, abbreviated BEDT-TTF or ET, have attracted much interest due to their rich phase diagrams [1,2]. Among these materials, the family of κ-$(ET)_2X$ salts, where κ refers to a specific arrangement of the ET molecules and X corresponds to a monovalent anion, stands out due to the realization of fascinating states of matter such as the Mott insulator, unconventional superconductors, or spin liquid [1–6]. In particular, the immediate vicinity of the superconducting phase to an antiferromagnetic Mott insulator suggests a deeper connection between two-dimensional organics and high-temperature cuprate superconductors [7].

Although superconducting κ-type charge-transfer salts have been investigated, for instance in studies of specific heat [3,8–12], surface impedance [13], thermal conductivity [14], millimeter-wave transmission [15], scanning tunneling spectroscopy (STS) [16–19], and elastic constants [20], no consensus about the symmetry of the superconducting pairing has been reached so far. Some of the experiments are in favor of s-wave symmetry [3,8,9], while other studies have proposed d-wave states with contradictory positions of the nodes in the superconducting order parameter [10–18]. Evidence for a mixed-symmetry order parameter was recently provided in Refs. [19,20]. Notably, evidence for a phase separation between different d-wave states has recently been reported in Ref. [18].

In theoretical approaches, the κ-$(ET)_2X$ family of materials is often described by a half-filled Hubbard model of $(ET)_2$ dimers on the anisotropic triangular lattice [21–25], which is equivalent to a square lattice model with an additional coupling along one of the diagonals. Many theoretical methods have been applied to the dimer-based Hubbard model, for instance the fluctuation-exchange approximation (FLEX) [26–29], the path-integral renormalization group [30], cluster dynamical mean-field theory [31–33], variational Monte Carlo [34–37], and exact diagonalization [38,39]. These studies do not agree entirely on all the details of the phase diagram, especially whether superconductivity is realized in the model or not. Those studies that do show superconductivity nevertheless agree, with the exception of Ref. [29], that it is of $d_{x^2-y^2}$-type as in high-temperature cuprate superconductors [40].

Although the triangular lattice Hubbard model has been remarkably successful in explaining the overall phase diagram [1,41,42] and also some more subtle physics [43] of κ-$(ET)_2X$ materials, the recent discovery of multiferroicity [44] in antiferromagnetic κ-$(ET)_2Cu[N(CN)_2]Cl$ and the still unresolved problem of superconducting-pairing symmetry [45,46] call for alternative approaches. In particular, the dimer model on the anisotropic triangular lattice is only an approximation with an *a priori* unclear range of applicability to the real lattice structure of κ-$(ET)_2X$ charge-transfer salts. In a seminal paper [47], Kuroki *et al.* investigated superconducting pairing, taking into account the realistic lattice structure, and in fact they found a phase transition between $d_{x^2-y^2}$- and d_{xy}-symmetric states when lowering the degree of dimerization. Other possible directions of future theoretical research beyond the dimer Hubbard model are outlined in Refs. [48–51].

In this work, building upon the idea by Kuroki *et al.*, we derive a set of realistic molecule-based low-energy models for superconducting κ-$(ET)_2X$ materials from *ab initio* density-functional-theory (DFT) calculations. After identifying the parameter region relevant for the real materials, we investigate the symmetry of the superconducting pairing in this model within a random-phase approximation (RPA) spin-fluctuation approach. Our results show that the position of many materials in the phase diagram is close to a phase-transition line between states with extended $s + d_{x^2-y^2}$ and d_{xy} pairing symmetry. Furthermore, we clarify that the customary dimer model not only fails in the limit of weak dimerization, but also when the in-plane anisotropy of hopping integrals becomes too large, which we find to be the case for all investigated materials.

*guterding@itp.uni-frankfurt.de

Finally, we simulate tunneling spectra in the superconducting state for selected cases, and we compare our findings to relevant experiments.

II. METHODS AND MODELS

A. *Ab initio* calculations and model Hamiltonian

We use *ab initio* density-functional-theory (DFT) calculations within an all-electron full-potential local orbital (FPLO) [52] basis to calculate the electronic band structure. For the exchange-correlation functional, we employ the generalized gradient approximation (GGA) [53]. All calculations are converged on $6\times6\times6$ k-point grids. We use crystal structures from Refs. [54–56]. In the case of Ref. [56], where crystal structures were measured for several temperatures, we use the data taken at 100 K.

In contrast to the customary dimer approximation, we model the κ-$(ET)_2^+$ layer, taking into account each individual ET molecule as a lattice site (see Fig. 1). Tight-binding parameters are obtained from projective molecular orbital Wannier functions as implemented in the FPLO code [57]. Therefore, the number of bands in the tight-binding model is equal to the number of ET molecules in the crystallographic unit cell. With the molecular Wannier function method, almost perfect representations of the DFT band structures can be obtained, and ambiguities from fitting procedures are avoided. The latter is especially important for many-body calculations based on the obtained low-energy Hamiltonians.

In the following model investigation, we only keep the four largest in-plane hopping elements (t_1,t_2,t_3,t_4) between ET molecules [see Fig. 1(a)]. The resulting hopping structure is a generalization of the Shastry-Sutherland lattice [58], which is reached in the limit of $t_2 = t_4$ and $t_3 = 0$. In cases in which the unit cell contains multiple κ-type layers, we discard all but one of the layers after the Wannierization procedure, because the interlayer coupling is negligible. In some of the investigated compounds, the crystal symmetry is lowered with respect to the high-symmetry orthorhombic space group *Pnma* of κ-$(ET)_2Cu[N(CN)_2]Br$, which leads to a small additional splitting of the hoppings t_i into $\tilde{t}_i$ and $\tilde{t}_i'$. For simplicity, this particular anisotropy is discarded in our study by averaging the hopping integrals as $t_i = (\tilde{t}_i + \tilde{t}_i')/2$. As a result, we obtain the kinetic part of a four-band Hamiltonian, which is 3/4-filled and of the same form for all materials investigated,

$$H_0 = \sum_{ij\sigma} t_{ij}(c_{i\sigma}^\dagger c_{j\sigma} + \text{H.c.}). \tag{1}$$

Alternatively, because ET molecules in a κ-type arrangement are quite strongly dimerized, it is popular to approximate the κ-$(ET)_2^+$ layer by dimers on an anisotropic triangular lattice, integrating out the intradimer degrees of freedom. The parameters of this dimer model can be calculated directly from the molecule model using geometric formulas [21],

$$t = (|t_2| + |t_4|)/2, \tag{2a}$$

$$t' = |t_3|/2. \tag{2b}$$

By convention, the dimer approximation uses the crystallographic unit cell containing two dimers [see Fig. 1(b)]. Therefore, the dimer-approximated Hamiltonian consists of two bands, which are half-filled. Note that based on the geometric formulas, any anisotropy between t_2 and t_4 of the molecule model is discarded when going from the molecule to the dimer model. With few exceptions [59], the dimer-approximated model nevertheless reproduces well the low-energy part of the original band structure. It has recently been demonstrated that improved estimates for dimer model parameters can be obtained by a Wannier function calculation [23,25,51].

The two-band dimer model can be unfolded to a one-band model by transforming to a unit cell of half the size and rotated by 45°. The so-obtained model is directly related to the square-lattice Hubbard model, but with an additional coupling along one of the diagonals. Results obtained in the one-band model are therefore rotated by 45° with respect to the physical Brillouin zone of organic charge-transfer salts, so that, e.g., different d-wave order parameters exchange their designation when going from one Brillouin zone to the other (see Fig. 2). Thus, the same physical order parameter that has d_{xy} symmetry in the realistic four-molecule–two-dimer unit cell [Fig. 2(b)] has $d_{x^2-y^2}$ symmetry in the model one-dimer–one-band unit cell [Fig. 2(c)]. In our study, we always work in the physical unit cell containing two dimers [Figs. 2(b) and 2(d)]. We refer to the small backfolded part of the Fermi surface close to the Brillouin zone boundary as the *elliptic* part of the Fermi surface, while we call those sheets running almost parallel to the k_y direction *quasi-one-dimensional*.

An overview of the unit cell and hopping paths for the molecule and dimer model is shown in Fig. 1. The resulting Hamiltonians in orbital space for all three cases are listed in Appendix A.

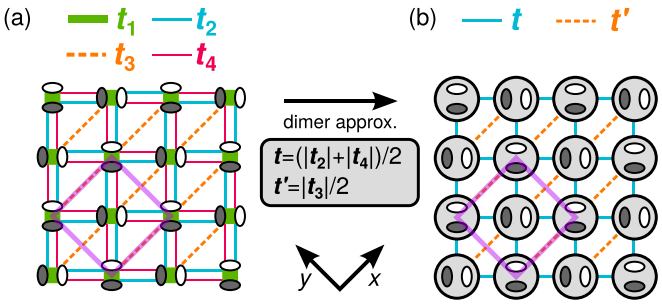

FIG. 1. (a) Molecule model of the κ-$(ET)_2^+$ layer. Individual ET molecules are represented by white and dark gray ellipsoids. The four dominant hopping integrals are (t_1,t_2,t_3,t_4). Note the pronounced asymmetry in magnitude between t_2 and t_4, which is indicated here by different line thicknesses. (b) Dimer-approximated κ-$(ET)_2^+$ layer. Two molecules are contracted into one dimer site indicated by a bold shaded circle. The intradimer hopping integral t_1 is integrated out, while t_2 and t_4 are averaged. Therefore, the dimer model is characterized by only two hopping parameters $\{t,t'\} = \{(|t_2| + |t_4|)/2, |t_3|/2\}$. In both subfigures, the unit cell considered in our work is indicated by a bold magenta-colored line.

B. RPA spin-fluctuation calculations

In κ-$(ET)_2X$ materials, there is strong evidence for antiferromagnetic spin fluctuations [60]. Therefore, we investigate the superconducting state of these materials based on a RPA spin-fluctuation approach in the singlet channel [61,62]. We

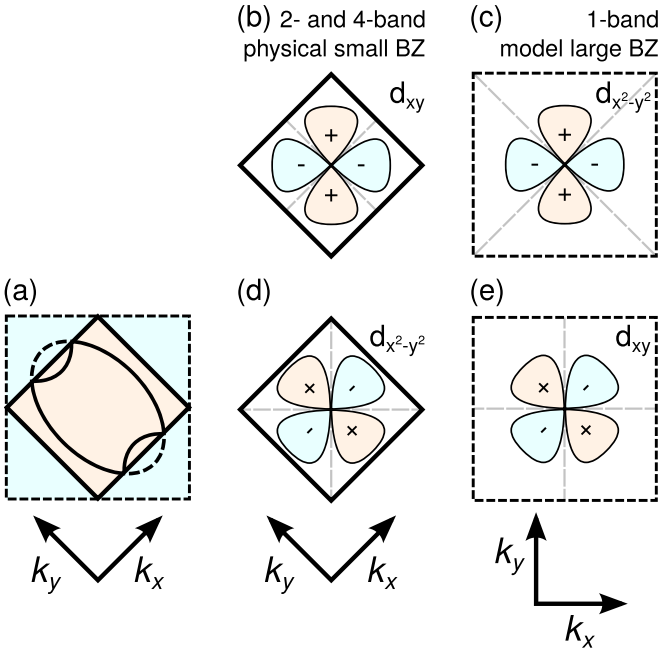

FIG. 2. (a) The inner bold lines show the Brillouin zone and the Fermi surface of a generic κ-$(ET)_2X$ material. The outer dashed lines show the Brillouin zone and the Fermi surface of the unfolded one-band dimer model. (b) d_{xy} order parameter in the physical Brillouin zone. Nodes are located in the x and y directions. (c) $d_{x^2-y^2}$ order parameter in the unfolded Brillouin zone. Nodes are located along the Brillouin-zone diagonals. The different designation is only due to a rotation of the coordinate axes by 45°. (d) $d_{x^2-y^2}$ order parameter in the physical Brillouin zone. (e) d_{xy} order parameter in the unfolded Brillouin zone.

have extended our implementation from single-site multiorbital models [63,64] to multi-site single-orbital models relevant for the materials discussed here. Compared to the FLEX approximation used in Ref. [47], our RPA method uses only states at the Fermi level and neglects the electronic self-energy correction. While this approximation prevents us from making quantitative statements about the superconducting transition temperature T_c, it reduces significantly the numerical cost compared to FLEX, so that we can calculate the momentum structure of the superconducting order parameter for numerous input parameter sets and with high angular resolution. Competing magnetically ordered or paramagnetic Mott insulating states are not investigated in our study. Furthermore, we do not investigate possible time-reversal symmetry-breaking superconducting states or spin-triplet pairing.

The low-energy Hamiltonian is given by the kinetic part H_0, derived with the Wannier-function method described above, and the intraorbital Hubbard interaction H_{int},

$$\begin{aligned} H &= H_0 + H_{\text{int}} \\ &= \sum_{ij\sigma} t_{ij}(c^\dagger_{i\sigma}c_{j\sigma} + \text{H.c.}) + \frac{U}{2}\sum_{i\sigma} n_{i\sigma}n_{i\bar{\sigma}}. \end{aligned} \tag{3}$$

Here, σ represents the spin and $n_{i\sigma} = c^\dagger_{i\sigma}c_{i\sigma}$. The sum over i runs over all ET sites in the unit cell. The interaction strength U is treated as a parameter. Note that the Coulomb repulsion on a dimer and the Coulomb repulsion on a molecule are not identical. At present, the role of intermolecular Coulomb repulsion is particularly unclear. The investigation of interaction terms beyond on-site repulsion is left for future studies.

We calculate the noninteracting static susceptibility χ^0, where matrix elements $a^l_\mu(\vec{k})$ resulting from the diagonalization of the initial Hamiltonian H_0 connect the orbital and the band space denoted by indices l and μ, respectively. The E_μ are the eigenvalues of H_0, and $f(E)$ is the Fermi function. N is the number of sites in the unit cell,

$$\begin{aligned} \chi^0_{l_1l_2l_3l_4}(\vec{q}) = -\frac{1}{N}\sum_{\vec{k},\mu,\nu} & a^{l_4}_\mu(\vec{k})a^{l_2*}_\mu(\vec{k})a^{l_1}_\nu(\vec{k}+\vec{q})a^{l_3*}_\nu(\vec{k}+\vec{q}) \\ & \times \frac{f(E_\nu(\vec{k}+\vec{q})) - f(E_\mu(\vec{k}))}{E_\nu(\vec{k}+\vec{q}) - E_\mu(\vec{k})}. \end{aligned} \tag{4}$$

In our calculation, both $\vec{q}$ and $\vec{k}$ run over uniform grids spanning the reciprocal unit cell. Temperature enters the calculation through the Fermi functions.

The fraction in Eq. (4) becomes problematic in numerical calculations, when the band energies E_ν and E_μ become degenerate. However, the expression can be rectified using l'Hospital's rule, which we use in practice when the magnitude of the denominator falls below a certain threshold (e.g., 10^{-7} eV). Here, β denotes the inverse temperature $\beta = (k_BT)^{-1}$,

$$\lim_{E_\nu \to E_\mu} \frac{f(E_\nu(\vec{k}+\vec{q})) - f(E_\mu(\vec{k}))}{E_\nu(\vec{k}+\vec{q}) - E_\mu(\vec{k})} = -\beta\frac{e^{\beta E_\nu}}{(e^{\beta E_\nu}+1)^2}. \tag{5}$$

The static spin and orbital susceptibilities ($\chi^{s,\text{RPA}}$ and $\chi^{c,\text{RPA}}$) are constructed in an RPA framework. Since the interaction term defined in Eq. (3) is local and we have only one orbital per lattice site, we can restrict the calculation to the diagonal elements of the susceptibility and use scalar equations for the RPA-enhanced susceptibilities,

$$\chi^{s,\text{RPA}}_L(\vec{q}) = \frac{\chi^0_L(\vec{q})}{1 - U\chi^0_L(\vec{q})}, \tag{6a}$$

$$\chi^{c,\text{RPA}}_L(\vec{q}) = \frac{\chi^0_L(\vec{q})}{1 + U\chi^0_L(\vec{q})}. \tag{6b}$$

Here, χ_L with $L = \{llll\}$ denotes the diagonal element of the susceptibility tensor associated with an ET site indexed by l. Note that this formulation allows us to treat multiple inequivalent ET sites in the unit cell, keeping the individual $\vec{q}$ dependence of their associated susceptibilities. Therefore, the symmetry of the susceptibility follows the symmetry of the ET layer in the crystallographic unit cell, which is important for checking the simplified four-parameter model against *ab initio* Hamiltonians, which can have monoclinic symmetry, as, e.g., in κ-$(ET)_2Cu(NCS)_2$, or even triclinic symmetry, as in κ-α'_1-$(ET)_2Ag(CF_3)_4(TCE)$.

The total spin susceptibility is given by the sum over all site-resolved contributions,

$$\chi^s(\vec{q}) = \frac{1}{2}\sum_L \chi^{s,\text{RPA}}_L(\vec{q}). \tag{7}$$

The pairing vertex in orbital space for the spin-singlet channel can be calculated using the fluctuation exchange approximation [65,66],

$$\Gamma_{l_1l_2l_3l_4}(\vec{k},\vec{k}') = \left[\tfrac{3}{2}U\chi^{s,\mathrm{RPA}}(\vec{k}-\vec{k}')U - \tfrac{1}{2}U\chi^{c,\mathrm{RPA}}(\vec{k}-\vec{k}')U + U\right]_{l_1l_2l_3l_4}. \quad (8)$$

In the pairing vertex, the momenta $\vec{k}$ and $\vec{k}'$ are restricted to the Fermi surface. As vectors $\vec{k}-\vec{k}'$ do not necessarily lie on the grid used in the calculation of the susceptibility $\chi^0(\vec{q})$, we interpolate the grid data linearly.

The pairing vertex in orbital space is transformed into band space using the matrix elements $a^l_\mu(\vec{k})$,

$$\Gamma_{\mu\nu}(\vec{k},\vec{k}') = \mathrm{Re}\sum_{l_1l_2l_3l_4} a^{l_1,*}_\mu(\vec{k})a^{l_4,*}_\mu(-\vec{k})[\Gamma_{l_1l_2l_3l_4}(\vec{k},\vec{k}')] \times a^{l_2}_\nu(\vec{k}')a^{l_3}_\nu(-\vec{k}'). \quad (9)$$

Finally, we solve the linearized gap equation by performing an eigendecomposition on the kernel and obtain the dimensionless pairing strength λ_i and the symmetry function $g_i(\vec{k})$,

$$-\sum_\nu \oint_{C_\nu}\frac{dk'_\parallel}{2\pi}\frac{1}{2\pi\, v_F(\vec{k}')}[\Gamma_{\mu\nu}(\vec{k},\vec{k}')]g_i(\vec{k}') = \lambda_i g_i(\vec{k}). \quad (10)$$

The integration runs over the discretized Fermi surface and $v_F(\vec{k})$ is the magnitude of the Fermi velocity.

For the computations presented in this paper, we evaluated the susceptibility $\chi^0(\vec{q})$ using 50×50 point grids for $\vec{q}$ and the integrated-out variable $\vec{k}$ [see Eq. (4)]. The inverse temperature in the susceptibility calculation is fixed to $\beta = 160/t_1$ for the molecule model and $\beta = 60/t$ for the dimer model. These values result in about the same effective temperature. The Fermi surface is determined by inverting linear interpolants for the band energies on a fine grid. For the models considered here, about 250 points on the Fermi surface are sufficient. The Hubbard repulsion parameter U is chosen in all calculations so that the leading eigenvalue in Eq. (10) is $\lambda = 0.99 \pm 0.001$. For most combinations of input parameters, this leads to a clear separation of the leading and the first subleading eigenvalue. The pairing symmetries corresponding to the leading and subleading eigenvalues do not change as a function of U.

C. Simulation of tunneling spectra in the superconducting state

The central quantity measured in the scanning tunneling spectroscopy (STS) experiments on superconductors is the local density of states (DOS) in the superconducting phase. Here we start from the standard Bardeen-Cooper-Schrieffer (BCS) theory for isotropic s-wave superconductors. A simple approximate extension allows us to treat realistic Fermi surfaces and unconventional pairing symmetries derived from the *ab initio* calculations combined with RPA spin-fluctuation theory as presented above.

To derive an approximation for the DOS of a superconductor, we start with the Hamiltonian for Cooper pairs with vanishing total momentum [67],

$$H = \sum_{k,\sigma}\epsilon_{k\sigma}c^\dagger_{k\sigma}c_{k\sigma} + \sum_{k,k'}U(k,k')c^\dagger_{k\uparrow}c^\dagger_{-k\downarrow}c_{-k'\downarrow}c_{k'\uparrow}. \quad (11)$$

The interaction can be treated in mean-field theory [$\delta(c^\dagger c^\dagger) = c^\dagger c^\dagger - \langle c^\dagger c^\dagger\rangle$], where terms quadratic in δ are neglected. The resulting Hamiltonian can be diagonalized using the Bogoliubov-Valatin transformation, which introduces quasiparticle creation and annihilation operators $\gamma^\dagger_{k\sigma}$ and $\gamma_{k\sigma}$. The quasiparticle excitation energies are given as $E_k = \sqrt{\epsilon_k^2 + |\Delta_k|^2}$, where $\Delta(k) = \sum_{k'}U(k,k')\langle c_{-k'\downarrow}c_{k'\uparrow}\rangle$.

The BCS Hamiltonian can be rewritten in terms of the quasiparticle creation and annihilation operators,

$$H_{\mathrm{BCS}} = \sum_{k,\sigma}E_k\gamma^\dagger_{k\sigma}\gamma_{k\sigma} + \sum_k\epsilon_k - \sum_{k,k'}U(k,k')\langle c^\dagger_{k\uparrow}c^\dagger_{-k\downarrow}\rangle\langle c_{-k'\downarrow}c_{k'\uparrow}\rangle. \quad (12)$$

The excitation spectrum of the quasiparticles E_k is gapped and defined only for positive energies. The density of states of quasiparticles in an isotropic s-wave superconductor can be calculated from the normal-state density of states $\rho(\epsilon)$ and the constant superconducting gap $\Delta_k = \Delta$,

$$\begin{aligned}\rho_{\mathrm{qp}}(E) &= \frac{1}{N}\sum_k\delta(E-E_k)\\ &= \int d\epsilon\,\rho_0(\epsilon)\frac{\sqrt{\epsilon^2+|\Delta|^2}}{\epsilon}\delta(\epsilon-\sqrt{E^2-|\Delta|^2})\\ &= \begin{cases}\rho_0(\sqrt{E^2-|\Delta|^2})\frac{E}{\sqrt{E^2-|\Delta|^2}}, & E>|\Delta|,\\ 0, & E<|\Delta|.\end{cases}\end{aligned} \quad (13)$$

The previous derivation assumed an isotropic gap and an energy dispersion of free electrons to identify the normal-state DOS ρ_0. For realistic electronic structure and anisotropic gap Δ_k this factorization of contributions is not easily possible due to the nontrivial momentum dependence of both functions:

$$\begin{aligned}\rho_{\mathrm{qp}}(E) &= \int d\epsilon\frac{1}{N}\sum_k\delta(\epsilon-\epsilon_k)\delta(|E|-\sqrt{\epsilon^2+|\Delta_k|^2})\\ &\neq \int d\epsilon\,\rho_N(\epsilon)\,\delta(|E|-\sqrt{\epsilon^2+|\Delta_k|^2}).\end{aligned} \quad (14)$$

However, in a widely used ansatz [68,69], the electrons with effective mass m^* are considered to be free, i.e., the Fermi surface is approximated by a concentric circle, and the gap only depends on the angle θ,

$$\rho_{\mathrm{qp}}(E) \approx \frac{1}{(2\pi)^2}m^*\mathrm{Re}\int d\theta\frac{|E|}{\sqrt{E^2-|\Delta(\theta)|^2}}. \quad (15)$$

We introduce in this expression a finite quasiparticle lifetime [70] by adding an imaginary part Γ to the quasiparticle excitation energies. This allows us to carry out calculations with finite angular resolution and facilitates comparison to experiment. Furthermore, we improve upon the circular integration by replacing it with a summation over the discretized realistic Fermi surface, and we drop the irrelevant prefactors

to obtain the final expression for the quasiparticle DOS in our study:

$$\rho_{\rm qp}(E) \propto \sum_{\vec{k}} {\rm Re} \frac{|E + i\Gamma|}{\sqrt{(E + i\Gamma)^2 - \Delta(\vec{k})^2}}. \quad (16)$$

In this form, the connection to the *ab initio* and RPA spin-fluctuation calculations is easily obtained: the vectors $\vec{k}$ in Eq. (16) all lie on the Fermi surface determined from the *ab initio* derived tight-binding model, and the gap $\Delta(\vec{k})$ on the Fermi surface can be substituted by the symmetry function $g_i(\vec{k})$ extracted from the RPA [Eq. (10)]. Note that the overall energy scale of the superconducting gap is not included in $g_i(\vec{k})$ because our formalism neglects the electronic self-energy and lacks a self-consistency condition. We checked that our approximation agrees well with a direct calculation of the quasiparticle spectrum based on Eq. (12), which is numerically more costly.

The quasiparticle DOS $\rho_{\rm qp}(E)$ corresponds to the local density of states (LDOS) measured in STS experiments. For a direct comparison, thermal smearing and additional effects such as electronic disorder might have to be taken into account [19,43,71].

III. RESULTS AND DISCUSSION

A. *Ab initio* calculations

Using *ab initio* density-functional-theory calculations and subsequent Wannier downfolding, we determine the parameter sets (t_1,t_2,t_3,t_4) corresponding to superconducting κ-(ET)$_2X$ materials with anions $X \in$ {Ag(CF$_3$)$_4$(TCE), I$_3$, Ag(CN)$_2\cdot$H$_2$O, Cu(NCS)$_2$, Cu[N(CN)$_2$](CN), Cu[N(CN)$_2$]Br}, as well as polymorphs κ-α_1'-(ET)$_2$Ag(CF$_3$)$_4$(TCE) and κ-α_2'-(ET)$_2$Ag(CF$_3$)$_4$(TCE), which also contain charge-ordered insulating α'-type layers. The calculated parameters are listed in Table I. In the case of (ET)$_2$Ag(CF$_3$)$_4$(TCE) polymorphs (TCE abbreviates 1,1,2-trichloroethane), we rely on a previous *ab initio* calculation with an identical setup [59]. The small asymmetry of hoppings due to the lowered symmetry in these materials is averaged out to obtain a four-parameter model. For the original models, see Ref. [59].

We observe that all materials fall into a narrow region of parameters: $t_1 \in$ [165,190] meV, $t_2 \in$ [95.6,119] meV, $t_3 \in$ [52.2,82.4] meV, and $t_4 \in$ [17.3,36.3] meV. Normalizing t_2, t_3, and t_4 with respect to t_1, this means all materials lie in the range $t_2/t_1 \in$ [0.538,0.661], $t_3/t_1 \in$ [0.289,0.404], and $t_4/t_1 \in$ [0.099,0.220]. Note the pronounced anisotropy between t_2 and t_4. These intervals of t_2/t_1, t_3/t_1, and t_4/t_1 obtained from the *ab initio* calculations determine the parameter ranges for our following model investigation.

We sorted the materials according to their superconducting transition temperature T_c, but we found no correlation of T_c with either t_1, t_2, t_3, or t_4. The ratios t_2/t_1, t_3/t_1, or t_4/t_1 are also not obviously connected to T_c.

B. Pairing symmetry in the dimer model

First, we apply the RPA spin-fluctuation formalism to the dimer model in the range $t'/t \in$ [0,1]. We evaluate the superconducting order parameter in fine steps of t'/t and compare the leading eigenfunctions. In all cases, we find that a d_{xy} state is the leading pairing symmetry.

Relating the dimer model back to the one-band model explained in Sec. II, the d_{xy} state we find is identical to the $d_{x^2-y^2}$ state of the square-lattice Hubbard model after unfolding the Brillouin zone (see Fig. 2). Typical superconducting κ-(ET)$_2X$ materials lie in the region $t'/t \lesssim 0.65$ [23,24,43], where a d_{xy} solution is to be expected, as the dimer model is basically a square lattice of hoppings t, perturbed by the additional diagonal coupling t'. The diagonal coupling t' breaks the C_4 symmetry of the underlying square lattice and gives the Fermi surface its elliptic shape, but the dominant terms in the Hamiltonian remain square-lattice-like. For a full account of possible pairing symmetries in the one-band Hubbard model on the square lattice, see Ref. [75].

An early theoretical study of the antiferromagnetic phase of κ-type materials concluded that the two molecules within a dimer carry the same spin and that the spins are flipped between neighboring dimers [22], giving rise to (π,π) magnetic order as in the parent compounds of high-temperature cuprate superconductors [40]. This result is consistent with our observation that a dimerized model gives a d_{xy} order parameter in the physical Brillouin zone, which becomes a $d_{x^2-y^2}$ symmetry in the unfolded zone of the one-band model (see Fig. 2), again emphasizing the deep connection between cuprates and quasi-two-dimensional organic superconductors.

TABLE I. Values of the molecule model parameters (t_1,t_2,t_3,t_4), also commonly denoted as (b_1,p,b_2,q), for selected superconducting κ-(ET)$_2X$ materials. All values are given in meV. Hopping integrals for the (ET)$_2$Ag(CF$_3$)$_4$ (TCE) family are averages of the parameters given in Ref. [59], where we used the same method and settings to calculate the parameters as in the present study. Crystal structures for these materials were taken from Refs. [54,55]. All other crystal structures are taken from Ref. [56]. The values for T_c are taken from Refs. [56,72–74]. In Ref. [43], models of the same form for nonsuperconducting κ-(ET)$_2X$ compounds are listed.

i	Material	T_c (K)	t_1	t_2	t_3	t_4	t_2/t_1	t_3/t_1	t_4/t_1	t_4/t_2
1	κ-(ET)$_2$Ag(CF$_3$)$_4$(TCE)	2.6	168	102	60.8	33.4	0.610	0.362	0.199	0.362
2	κ-(ET)$_2$I$_3$	3.6	180	119	52.2	31.7	0.661	0.289	0.176	0.266
3	κ-(ET)$_2$Ag(CN)$_2\cdot$H$_2$O	5.0	185	104	60.4	23.6	0.567	0.326	0.173	0.305
4	κ-α_1'-(ET)$_2$Ag(CF$_3$)$_4$(TCE)	9.5	166	97.6	65.8	35.3	0.588	0.396	0.213	0.362
5	κ-(ET)$_2$Cu(NCS)$_2$	10.4	190	102	82.4	17.5	0.538	0.387	0.092	0.171
6	κ-α_2'-(ET)$_2$Ag(CF$_3$)$_4$(TCE)	11.1	165	98.4	66.7	36.3	0.596	0.404	0.220	0.369
7	κ-(ET)$_2$Cu[N(CN)$_2$](CN)	11.2	175	100	78.5	17.3	0.574	0.344	0.099	0.172
8	κ-(ET)$_2$Cu[N(CN)$_2$]Br	11.6	177	95.6	60.0	36.2	0.541	0.339	0.205	0.379

We would also like to note that the authors of Ref. [18], referring to the physical Brillouin zone, invoked a d_{xy} superconducting symmetry close to insulating patches and a $d_{x^2-y^2}$ state in the bulk to explain the findings of their STS study on deuterated κ-(ET)$_2$Cu[N(CN)$_2$]Br. As the antiferromagnetic insulating state is dimerized (see Ref. [22]), the dimer approximation naturally applies and gives a d_{xy} order parameter in accordance with the experimental observation. What remains to be answered in an approach beyond the dimer model, as presented in the next sections, is why the superconducting order parameter of the bulk is $d_{x^2-y^2}$.

C. Pairing symmetry in the molecule model

The obvious step for going beyond the dimer model is to use the original crystal lattice, i.e., the molecule model explained above (see Fig. 1). To compare the results of the molecule model to those of the dimer model, we make the following consideration: via the geometric Eq. (2), the four-parameter molecule model is mapped onto a two-parameter dimer model. With this procedure we are left with two adjustable parameters in the molecule model whose variation discloses important features of the systems, not captured in the resulting dimer model, which remains unchanged. These adjustable parameters are the degree of dimerization $t_1/\max(t_2,t_3,t_4)$ and the in-plane anisotropy t_4/t_2.

The degree of dimerization obviously decides whether the dimer approximation applies to a material or not. Its influence on the superconducting pairing was quantified by Kuroki *et al.*, who found a transition to a $d_{x^2-y^2}$ state in the physical Brillouin zone at low dimerization (see Ref. [47]).

Less obvious is how this $d_{x^2-y^2}$ state emerges from the underlying hopping structure and how important the anisotropy between t_2 and t_4 is for the pairing state. To investigate these issues, we construct a series of molecule models with a fixed value of $t_3/t_1 = 0.333$, and we vary the ratio t_4/t_2 in the range [0,1] (for the values realized in real materials, see Table I). We fix the sum of t_2 and t_4 so that the molecule models correspond to the same dimer model $t_3/(t_2+t_4) = t'/t = 0.6$. The maximum value of t_2 is therefore $t_2^{\max} = 0.556$ and its minimum value is $t_2^{\min} = 0.278$. As t_4 is increased, the in-plane anisotropy decreases and the dimerization defined as $t_1/\max(t_2,t_3,t_4)$ increases.

In Fig. 3, we show the spin susceptibilities and leading pairing symmetries in the molecule model as a function of t_4/t_2 compared to the associated dimer model. In the isotropic limit $t_4/t_2 = 1$ we find a d_{xy}-symmetric state, similar to the one found in the dimer model [compare Figs. 3(d) and 3(e)]. Upon lowering t_4/t_2, the maxima of the superconducting gap shift toward the position where the nodes in a d_{xy}-symmetric state are and additional nodes appear on the quasi-one-dimensional part of the Fermi surface close to $(\pm\pi,0)$. As this shift is equivalent to a rotation by 45°, the state with eight nodes can be expected to have a significant $d_{x^2-y^2}$ contribution. In the limit of $t_4 \ll t_2$, the additional set of nodes on the quasi-one-dimensional part of the Fermi surface vanishes [see Fig. 3(a)]. The remaining four nodes are situated close to the Brillouin-zone boundary, where the smaller elliptic part of the Fermi surface is folded back. The details of the pairing symmetry are discussed further below. In what follows, we investigate the origin of the gap maxima shifts.

As an example, we show in Fig. 4 how extrema of the gap magnitude with opposite sign appear where parts of the Fermi surface can be connected by a wave vector $\vec{q}$ that shows a peak in the spin susceptibility. Note that in Fig. 4 the Brillouin zone is shifted by a vector (π,π), because the relevant vectors $\vec{q}$ connect pieces of the Fermi surface across the boundaries of the Brillouin zone used in Fig. 3.

Now we come back to the discussion of the results presented in Fig. 3. At $t_4/t_2 = 0$, peaks appear at $\vec{q}_1 \approx (\pm 0.7\pi, 0)$ and $\vec{q}_2 \approx (\pm\pi/2, \pm\pi)$, the dominant contribution to the spin susceptibility being the peak at $\vec{q}_2$. As t_4/t_2 is increased, the

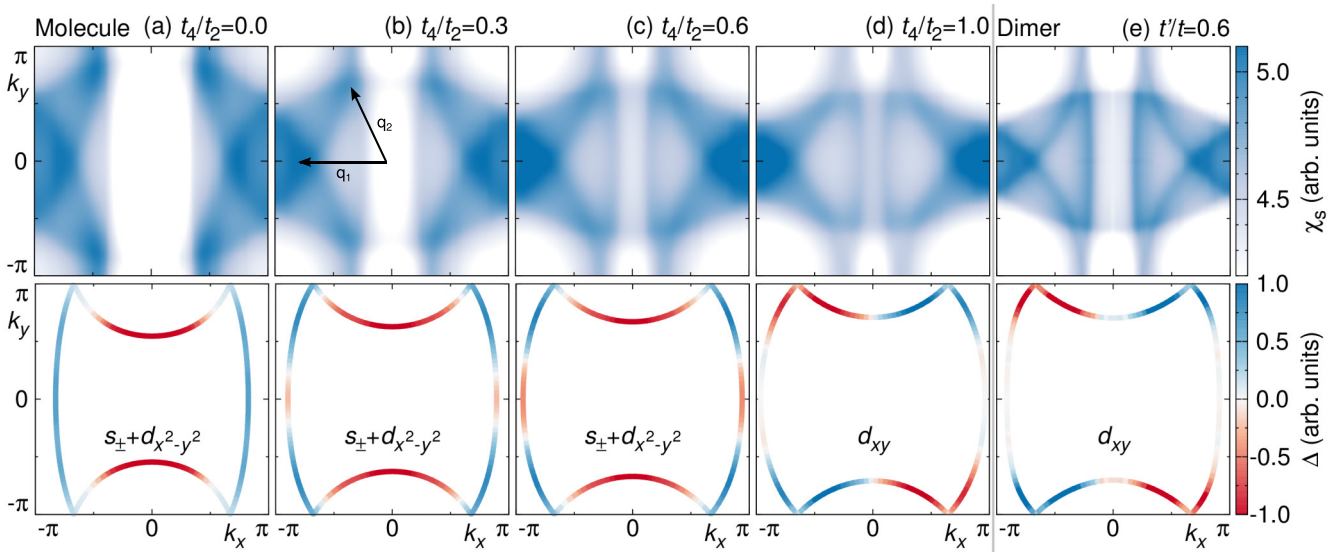

FIG. 3. Comparison of molecule models (a)–(d) with different ratios of t_4/t_2, which all correspond to the same dimer model (e) with $t'/t = 0.6$. The top panel shows the spin susceptibilities, where arrows $\vec{q}_1$ and $\vec{q}_2$ indicate the main features, while the bottom panel shows the leading eigenfunction of the superconducting gap equation on the Fermi surface. In the molecule models $t_3/t_1 = 0.333$ is fixed, while the ratio of t_4/t_2 is varied under the condition $t_3/(t_2+t_4) = t'/t = 0.6$.

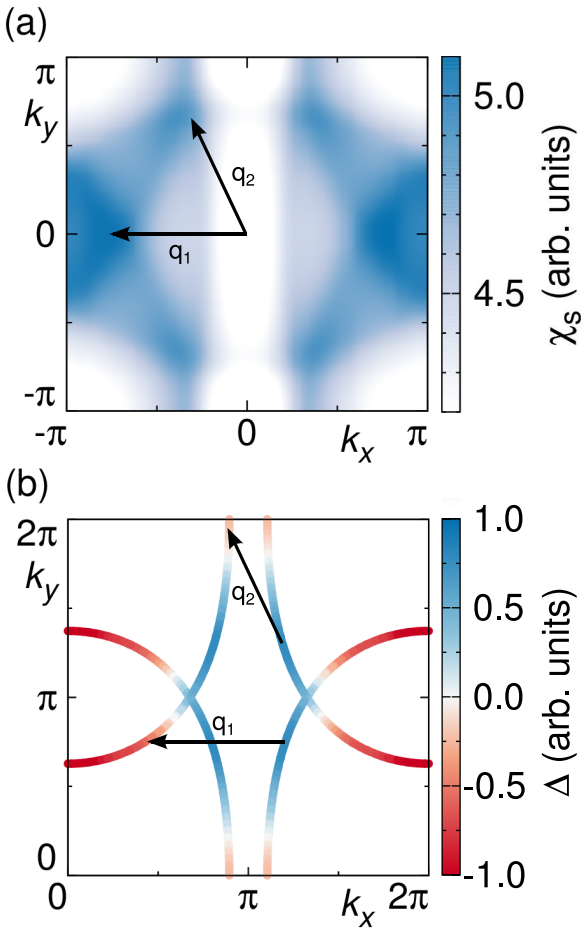

FIG. 4. (a) Spin susceptibility of the molecule model at $t_2/t_1 = 0.417$, $t_3/t_1 = 0.333$, and $t_4/t_1 = 0.139$, with arrows $\vec{q}_1$ and $\vec{q}_2$ indicating the main features. The data shown are the same as in Fig. 3(b). (b) Superconducting gap function on the Fermi surface for the same parameter values as in (a). Vectors $\vec{q}_1$ and $\vec{q}_2$ are the same as in (a) and connect parts of the Fermi surface with different signs of the gap. Note that the plot range of the Brillouin zone is shifted by a vector (π,π) compared to Fig. 3.

position of $\vec{q}_1$ remains about the same, while $\vec{q}_2$ shifts toward $(\pm\pi/4, \pm\pi/2)$ and decreases in intensity. At $t_4/t_2 = 1$, the peak at $\vec{q}_1$ becomes the dominant contribution to the spin susceptibility. As we do not work in the limit of infinite dimerization, even the case $t_4/t_2 = 1$ does not reproduce the dimer model spin susceptibility exactly. The similarities are, however, apparent.

These peak shifts in the spin susceptibility are reflected in the pairing symmetry: the gap maxima of different sign in the d_{xy} symmetry are separated by a wave vector $\vec{q}_1$, while $\vec{q}_2$ is responsible for the sign change between the upper and lower half of the elliptic Fermi surface. Furthermore, $\vec{q}_2$ enforces an enlarged nodal region close to $(\pm\pi,0)$, since it would otherwise connect parts of the Fermi surface with the same sign of the gap. In the intermediate region of t_4/t_2, $\vec{q}_2$ connects the one-dimensional (1D) parts of the Fermi surface, where it induces an additional set of nodes. The large gap on the elliptic part of the Fermi surface is connected to the 1D sheets by $\vec{q}_1$. The shift of the vertical lines in the susceptibility, which widen toward $k_x \approx \pm\pi/2$, merely reflect the changing shape of the Fermi surface. For $t_4 \ll t_2$, the additional set of nodes on the 1D sheets vanishes, because they are no longer connected by $\vec{q}_2$, which now instead points from the 1D sheet to the elliptic parts just like q_1. This consideration shows that the pairing-symmetry transition in the molecule model is driven by a peculiar competition between $\vec{q}_1$ and $\vec{q}_2$ nesting vectors.

Now we connect the structure of the susceptibility and the superconducting pairing to the underlying lattice model. The feature at $\vec{q}_1$ is obviously connected to the t_3 hopping parameter, since it is the only hopping exclusively in the x direction (compare Fig. 1). All other t parameters can only be responsible for a four-peak structure, as they occur pointing along both diagonals of the physical unit cell. The influence of the competition between t_2, t_3, and t_4 on the feature at $\vec{q}_2$ is, however, hard to quantify directly. Therefore, we decompose the superconducting order parameter in terms of extended s- and d-wave basis functions f_i appropriate for a square-lattice geometry. For each of the d-wave basis functions, we also take into account the associated extended s-wave function, because we expect that a significant extended s-wave component could mix with the d-wave states to accommodate the orthorhombicity of the model:

$$f_{s_1}(\vec{k}) = \cos k_x + \cos k_y, \tag{17a}$$

$$f_{d_{x^2-y^2}}(\vec{k}) = \cos k_x - \cos k_y, \tag{17b}$$

$$f_{s_2}(\vec{k}) = \cos k_x \cdot \cos k_y, \tag{17c}$$

$$f_{d_{xy}}(\vec{k}) = \sin k_x \cdot \sin k_y. \tag{17d}$$

Rotated into the Brillouin zone of κ-type materials, gap functions $f_{d_{xy}}$ and f_{s_2} are to be expected from antiferromagnetic exchange along squarelike bonds (t_2, t_4), while f_{s_1} and $f_{d_{x^2-y^2}}$ correspond to exchange paths along diagonal bonds (t_3); see Fig. 5.

We fit the pairing symmetries calculated from the RPA to a linear combination of the previously defined pairing symmetries, and we determine their relative contributions c_i,

$$\tilde{g}(\vec{k}) = c_{s_1} f_{s_1} + c_{d_{x^2-y^2}} f_{d_{x^2-y^2}} + c_{s_2} f_{s_2} + c_{d_{xy}} f_{d_{xy}}. \tag{18}$$

For the d_{xy} state, we find $c_{d_{xy}} = 1$ and all other contributions zero, i.e., except for the not well-reproduced extended nodal

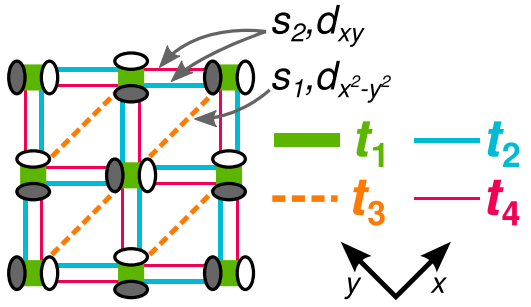

FIG. 5. Hopping structure in the molecule model for the κ-$(ET)_2^+$ layer. The dark gray arrows indicate the connection between hopping parameters and the symmetry functions appearing in the solution of the superconducting gap equation.

region close to $(\pm\pi,0)$, the dimer model and the molecule model at $t_4/t_2 \lesssim 1$ are dominated by the square-lattice physics of t and t_2,t_4, respectively. For the $d_{x^2-y^2}$-like solution at $t_4 \ll t_2$ we find negligible contributions from f_{s_1} and $f_{d_{xy}}$, dominant f_{s_2}, and subdominant $f_{d_{x^2-y^2}}$. For increasing t_4/t_2, the ratio of coefficients $c_{d_{x^2-y^2}}/c_{s_2}$ decreases, i.e., the square-lattice physics becomes dominant when the asymmetry between t_2 and t_4 is removed. Using the symmetry functions f_i, all details of the superconducting gap in the $d_{x^2-y^2}$-like state including the additional nodes can be reproduced by Eq. (18).

Our findings provide a clear picture of the pairing competition in the molecule model: in the realistic region of parameters, where the dimerization measured by $t_1/\max(t_2,t_3,t_4)$ and the anisotropy of t_2 and t_4 are finite, the competition of squarelike (t_2, t_4) and diagonal (t_3) hopping realizes a unique linear combination of functions $f_{d_{x^2-y^2}}$ and f_{s_2} as the leading pairing symmetry. We refer to this linear combination as $s_\pm + d_{x^2-y^2}$, or extended $s + d_{x^2-y^2}$. The s-wave contribution is equivalent to the $s_\pm$ pairing state believed to be realized in iron-based superconductors (see, e.g., Ref. [76]), and it has been overlooked entirely in the literature on quasi-two-dimensional organic charge-transfer salts. When the lattice becomes more squarelike ($t_4 \lesssim t_2$), i.e., the molecule model approaches the dimer limit, the d_{xy} symmetry known from the dimer model takes over. In other words, in the context of realistic modeling of κ-type materials, the d_{xy} symmetry found in the dimer model ($d_{x^2-y^2}$ in the unfolded one-band model) is mostly an artifact of the underlying approximation to the real lattice structure [Eq. (2)].

Finally, we checked our results obtained with the four-parameter molecule model against the original hopping structure obtained from projective Wannier functions, which includes longer-range processes. As expected, the differences induced by the distance cutoff and parameter averaging are negligible.

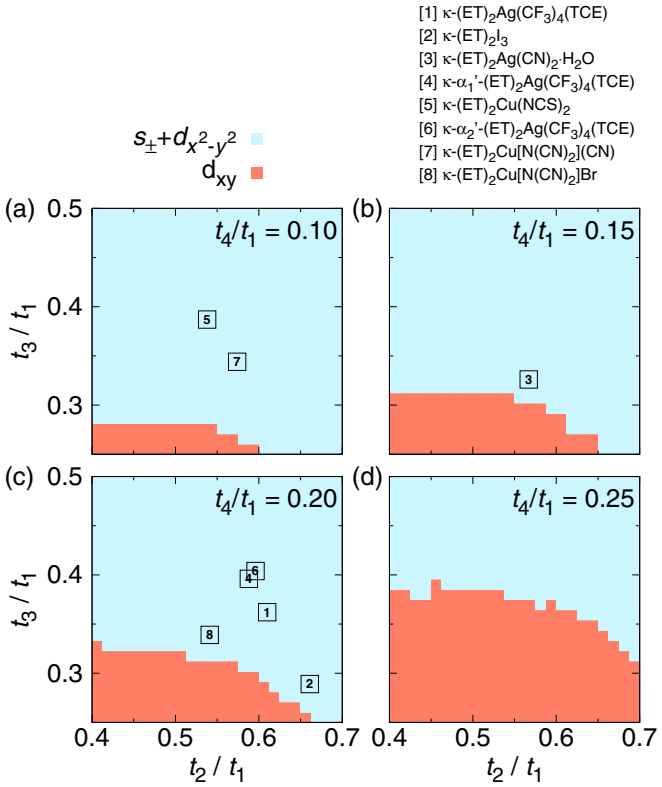

FIG. 6. Superconducting phase diagram of the individual molecule model. Different symmetries of the superconducting order parameter are color-coded. A d_{xy} symmetry of the pairing interaction is favored when the orthorhombicity of the system is small, i.e., when $t_4 \lesssim t_2$ and $t_3 \ll t_2$. In the rest of the phase diagram, an extended $s + d_{x^2-y^2}$ symmetry prevails. The numbered symbols correspond to the location of real materials in the phase diagram, enumerated as in Table I. Materials were sorted into the subplot to which their true value of t_4/t_1 is closest.

D. Pairing symmetry phase diagram of the molecule model

To complete our study of the pairing symmetry competition, we investigated the leading pairing symmetry of the molecule model as a function of t_2/t_1, t_3/t_1, and t_4/t_1 in the range of parameters realized in actual superconducting κ-type materials.

In Fig. 6 we show the obtained phase diagram, which consists of a d_{xy}-symmetric phase at low t_2/t_1 and t_3/t_1, while the rest of the phase diagram shows an $s_\pm + d_{x^2-y^2}$ state. The consecutively numbered symbols in Fig. 6 correspond to the position of real materials as listed in Table I within this phase diagram. As we scanned the phase diagram several times for different fixed t_4/t_1, materials were sorted into the cut with the closest value of t_4/t_1.

At low t_2/t_1 the phase boundary is almost horizontal, i.e., independent of the precise value of t_2/t_1. For larger values of t_2/t_1, the model becomes more asymmetric with respect to t_2 and t_4, and a smaller diagonal coupling t_3 is sufficient to drive the system into the $s_\pm + d_{x^2-y^2}$ state. The size of the d_{xy}-symmetric region is obviously determined by the value of t_4/t_1 as explained in the preceding section.

In the numerical calculations, we observed that the leading two pairing symmetries are almost degenerate in a broad parameter region. This is to be expected, because the $s_\pm + d_{x^2-y^2}$ state emerges precisely as a compromise between two different nesting vectors, of which one rather fits to a pure d_{xy} symmetry. To clarify this degeneracy, we calculated the eigenvalues of the leading and subleading solutions of the gap equation at fixed t_2/t_1 and t_3/t_1 and varied t_4/t_2 in the range [0,1]. Figure 7 shows the eigenvalues of both possible pairing states as a function of the in-plane anisotropy t_4/t_2. We observe a pronounced asymmetry: While the d_{xy} state is competitive even for low values of t_4/t_2, the $s_\pm + d_{x^2-y^2}$ quickly becomes irrelevant when approaching the isotropic case ($t_4/t_2 = 1$).

Finally, based on our parameter estimates, all materials investigated lie in the $s_\pm + d_{x^2-y^2}$ region of the phase diagram. Materials particularly close to the phase-transition line are κ-$(ET)_2I_3$, κ-$(ET)_2Ag(CN)_2 \cdot H_2O$, and κ-$(ET)_2Cu[N(CN)_2]Br$. These can be expected to realize the $s_\pm + d_{x^2-y^2}$ order parameter with eight nodes. Evidence for eight-node mixed-symmetry superconductivity has recently been found in Ref. [19].

When materials are close to the phase-transition line, small changes of the hopping parameters might drive them into the d_{xy} state, which is always present as a subdominant pairing symmetry. For such local changes of parameters, for instance

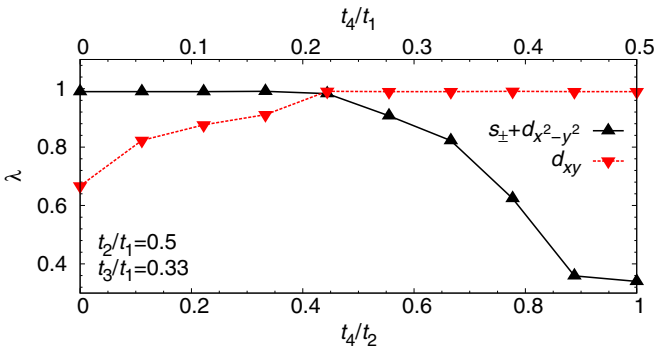

FIG. 7. Eigenvalues of the gap equation for $s_\pm + d_{x^2-y^2}$ and d_{xy} pairing symmetries as a function of the in-plane anisotropy t_4/t_2. The isotropic case is realized for $t_4/t_2 = 1$. Only t_4 was varied. The other parameters were fixed to $t_2/t_1 = 0.5$ and $t_3/t_1 = 0.33$.

lattice defects [77,78] or disorder of molecular conformations could be responsible. In Ref. [43] we have shown that different conformations of ET molecules result in decidedly different ratios of t_4/t_2. The degree of conformational disorder can be controlled experimentally by adjusting the sample cooling rate [79,80].

In Ref. [22], a square-lattice-like antiferromagnetic order was found for the insulating state of κ-type materials. Therefore, we expect significant competition between antiferromagnetism and d_{xy}-symmetric superconductivity, while the $s + d_{x^2-y^2}$-symmetric state is realized farther away from the magnetically ordered insulating phase. Within this picture, recent results by Oka *et al.* [18], who interpreted their experiment in terms of patches with a d_{xy} order parameter and a $d_{x^2-y^2}$-symmetric bulk, can be qualitatively explained.

At this point, we would like to point out that most experimental studies assume a four-node d-wave order parameter upon data analysis, which excludes from the start the detection of the $s_\pm$ component we found. In particular, the realization of the $s_\pm + d_{x^2-y^2}$ state with eight nodes that lie along the diagonals and close to the crystallographic axes may explain the considerable disagreement in the experimental literature regarding the node positions.

E. Simulation of scanning tunneling spectroscopy

Most transport experiments on κ-$(ET)_2X$ materials have proven to be difficult to interpret and could not resolve the symmetry of the superconducting pairing so far. However, recent improvements in sample preparation for low-temperature scanning tunneling spectroscopy (STS) experiments have allowed for progress toward a resolution of the superconducting order parameter [18,19,71].

Therefore, in this section we simulate tunneling spectra in the superconducting state for molecule model parameters $t_2/t_1 = 0.4375, t_4/t_1 = 0.1$, and various values of t_3/t_1: a four-node $s_\pm + d_{x^2-y^2}$ state is obtained for $t_3/t_1 = 0.5$, an eight-node $s_\pm + d_{x^2-y^2}$ state for $t_3/t_1 = 0.3475$, and d_{xy} for $t_3/t_1 = 0.25$. We employ the representation of the superconducting gap in terms of symmetry functions introduced in Eq. (18), which we multiply with a prefactor $\Delta_0 = 10$ meV to obtain a spectrum with a reasonable energy scale. The gap on the Fermi surface is then given by $\Delta(\vec{k}) = \Delta_0 \tilde{g}(\vec{k})$. We use this expression together with Eq. (16) to calculate the quasiparticle density of states $\rho_{\rm qp}$, which corresponds to the local density of states (LDOS) observed in STS experiments. The finite quasiparticle lifetime is modeled by $\Gamma = 0.07$ meV. In the d_{xy} case, we ignore the small anisotropy found in the RPA calculation.

In Fig. 8 we show (i) the obtained gap on the Fermi surface, (ii) the magnitude of the gap versus angle measured from the k_x direction, and (iii) the simulated tunneling spectrum for the three cases investigated.

The magnitude of the gap versus the angle is distributed anisotropically on the Fermi surface [Figs. 8(a)–8(c), top panel]. Maxima of the gap magnitude are indicated by arrows labeled with capital letters, while nodes in the gap are indicated by arrows labeled with greek letters. The global maximum of the gap magnitude (labeled A or D) resides in all cases on the elliptic part of the Fermi surface, while the second largest maximum (labeled B or E) is located on the quasi-one-dimensional part. A third smallest maximum (labeled C) is possible on the quasi-1D sheet. In the d_{xy} case, the nodes labeled γ appear in addition to the expected set of nodes δ, because the Fermi surface touches the Brillouin zone boundary. The γ nodes lead to the second maximum (labeled E) of the gap magnitude [Figs. 8(a)–8(c), middle panel], but they are otherwise irrelevant for the low-energy physics. As the three possible gap structures share two maxima of slightly different size, the simulated quasiparticle DOS looks quite generic [Figs. 8(a)–8(c), bottom panel]. A two-peak structure is observed far away from the Fermi level, which corresponds to the energy values of the two largest maxima in the gap magnitude.

Important differences are revealed, however, at low energies: the d_{xy} state is featurelessly V-shaped [Fig. 8(c), bottom panel], while the spectrum of the eight-node state has an additional peak close to 2 meV [Fig. 8(b), bottom panel], which is linked to the small gap (labeled C) on the quasi-1D sheet. This leads to an outer and an inner V-shape with different slopes. For the four-node $s_\pm + d_{x^2-y^2}$ state we observe a peculiar dip around 1 meV in the quasiparticle spectrum [Fig. 8(a), bottom panel]. This corresponds to the minimum value of the gap magnitude on the quasi-one-dimensional part of the Fermi surface. Inside of this dip, a V-shaped region emerging from the β nodes is again observed.

We emphasize that our predictions are to be taken as qualitative, not quantitative, regarding the overall energy scale and the relative gap sizes. The main features explained above, however, are robust. The detection of such low-energy structures is certainly not an easy task, but we believe it will be possible with state-of-the-art equipment and proper sample preparation.

IV. CONCLUSIONS

In summary, we investigated the superconducting state of κ-$(ET)_2X$ charge-transfer salts in an individual molecule model based on a combination of *ab initio* density-functional theory and random-phase approximation spin-fluctuation calculations. We obtained kinetic parameters of the molecule Hamiltonian for eight superconducting κ-type materials using

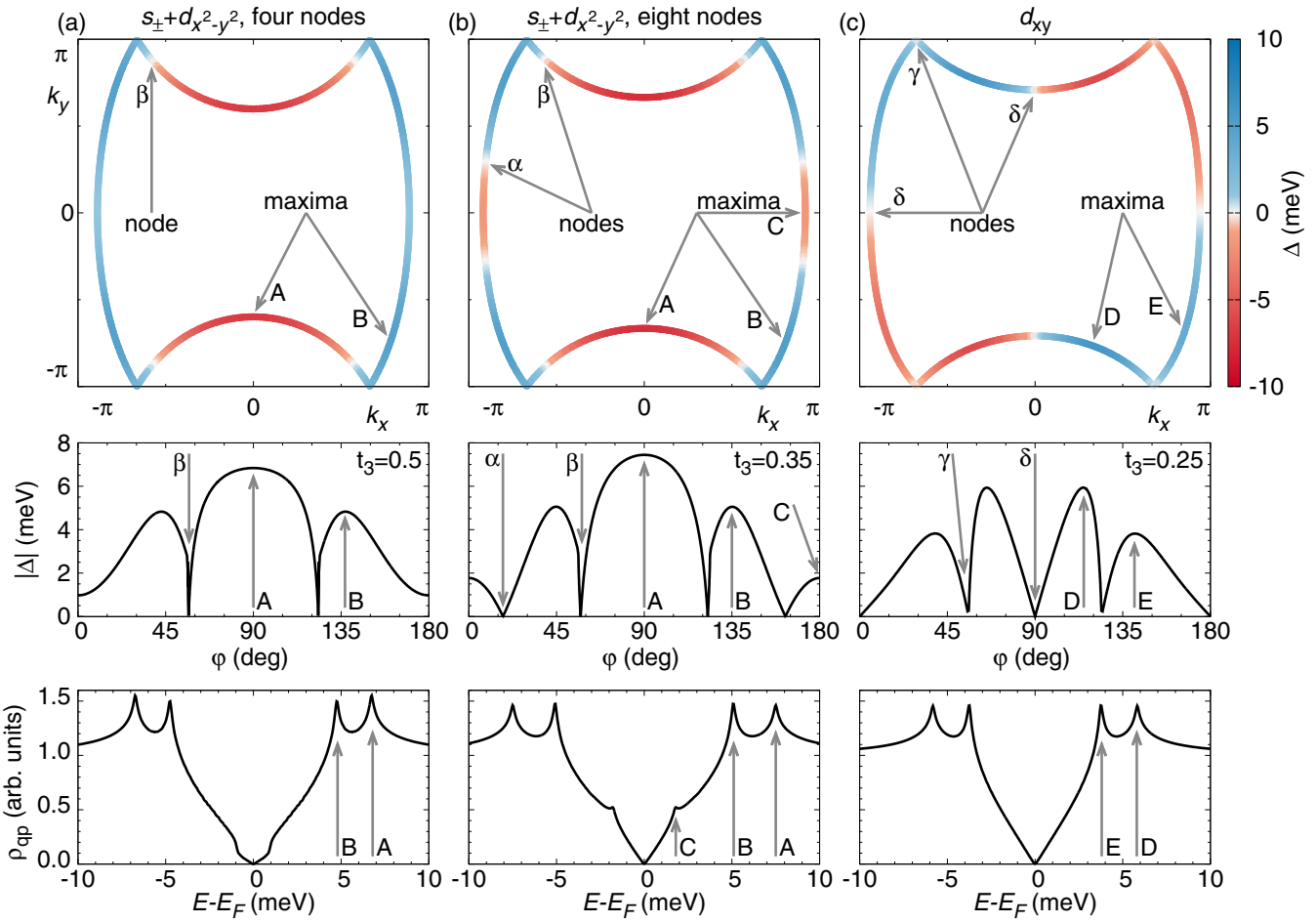

FIG. 8. Gap function on the Fermi surface (top panel), magnitude of the gap function vs angle measured with respect to the k_x direction (middle panel), and simulated quasiparticle density of states in the superconducting state (bottom panel). In all cases, we assumed an energy scale $\Delta_0 = 10$ meV. Only t_3/t_1 is varied. Other parameters are fixed to $t_2/t_1 = 0.4375$ and $t_4/t_2 = 0.1$. Maxima of the superconducting gap magnitude are labeled with upper-case letters. Nodes of the superconducting order parameter are labeled with greek letters. All nodes and maxima not labeled explicitly are symmetry-equivalent to the labeled ones. Column (a) shows the case of $s_\pm + d_{x^2-y^2}$ symmetry with four nodes ($t_3/t_1 = 0.5$). Column (b) shows the results for $s_\pm + d_{x^2-y^2}$ symmetry with eight nodes ($t_3/t_1 = 0.3475$). Column (c) shows the d_{xy} case ($t_3/t_1 = 0.25$).

projective Wannier functions. We found that the superconducting order parameter in a realistic molecule model is different from the one in the usual dimer-approximated Hamiltonian for all investigated materials. The superconducting phase diagram of the molecule description is dominated by an extended $s + d_{x^2-y^2}$ symmetry that emerges from the competition between squarelike and diagonal hopping processes on the original κ-type lattice, while the physics of the dimer model is reproduced also for finite dimerization in the limit of isotropic parameters, $t_4 \lesssim t_2$. The anisotropy of squarelike hoppings t_2 and t_4 is, however, not negligible in real materials. For precisely this reason, the dimer approximation does not apply to superconducting κ-$(ET)_2X$ charge-transfer salts. It overestimates the importance of square-lattice physics through the averaging contained in the geometric formulas, which are exact only in the limit of infinite dimerization.

Furthermore, the $s_\pm + d_{x^2-y^2}$ state, which features nodes both along the crystallographic axes and the Brillouin zone diagonals, might explain the multitude of contradictory experimental results regarding the nodal positions. We also simulated tunneling spectroscopy experiments for all nodal configurations encountered in our phase diagram. The difference between those pairing states unfortunately manifests itself only at very low energies, making experimental detection difficult, but not impossible. Based on the *ab initio* calculated model parameters, we found that the well-studied material κ-$(ET)_2Cu[N(CN)_2]Br$ is situated near the phase-transition line between $s_\pm + d_{x^2-y^2}$ and d_{xy} superconducting states, which supports the interpretation of recent scanning tunneling spectroscopy experiments.

A question unanswered by our study is why superconducting transition temperatures among quasi-two-dimensional charge-transfer salts can differ by more than a factor of 4. As there is no obvious connection between T_c and the parameters of the kinetic Hamiltonian, a method that can qualitatively reproduce the ordering of transition temperatures in real materials is required to elucidate this issue.

In conclusion, we believe that a significant part of the physics in quasi-two-dimensional charge-transfer salts has unfortunately been overlooked so far, because theory has

adhered to the dimer model for too long, and too many experiments have been interpreted based on a dichotomy of d_{xy} and $d_{x^2-y^2}$ states, which is inappropriate for the orthorhombic lattice realized in κ-$(ET)_2X$ materials.

It is an interesting open question whether the magnetic, insulating, and possible quantum spin-liquid states known from the anisotropic triangular lattice are also present in the molecule model. The investigation of these phases is left for future studies.

ACKNOWLEDGMENTS

The authors acknowledge fruitful discussions with Ryui Kaneko, Stephen M. Winter, Andreas Kreisel, and Peter J. Hirschfeld. This work was supported by the German Research Foundation (Deutsche Forschungsgemeinschaft) under Grant No. SFB/TR 49. Calculations were performed on the LOEWE-CSC and FUCHS supercomputers of the Center for Scientific Computing (CSC) in Frankfurt am Main, Germany.

APPENDIX: MATRIX ELEMENTS OF THE KINETIC HAMILTONIANS

For completeness, we list the kinetic part of the dimer model in one- and two-band representation, as well as the kinetic part of the four-band molecule model. We denote the unit-cell parameters in the x and y directions as a and b, respectively. The multiband Hamiltonians are given as matrix elements $\langle i|H_{\rm hop}|j\rangle$, where states $|i\rangle$ denote the orbitals living on a dimer/molecule with site index i. Only unique matrix elements are listed. The rest of the elements are generated by using $\langle i|H_{\rm hop}|j\rangle = \langle j|H_{\rm hop}|i\rangle^*$. In all models, there is only one orbital per lattice site.

To obtain the correct electron filling, one has to introduce a chemical potential μ, so that $H_0 = H_{\rm hop} - \mu \sum_{i\sigma} c^\dagger_{i\sigma} c_{i\sigma}$ is half-filled for the dimer model in either representation and 3/4-filled for the molecule model.

The single-band representation of the dimer model is given by

$$H_{\rm hop}(\vec{k}) = 2t[\cos(k_x a) + \cos(k_y b)] + 2t'[\cos(k_x a)\cos(k_y b) - \sin(k_x a)\sin(k_y b)]. \quad \text{(A1)}$$

The two-band representation of the dimer model can be written as

$$\langle 0|H_{\rm hop}|0\rangle = \langle 1|H_{\rm hop}|1\rangle = 2t'\cos(k_x a), \quad \text{(A2a)}$$

$$\langle 0|H_{\rm hop}|1\rangle = 2t(1 + e^{ik_x a} + e^{ik_y b} + e^{ik_x a}e^{ik_y b}). \quad \text{(A2b)}$$

The four-band molecule model is given by

$$\langle 0|H_{\rm hop}|1\rangle = t_1 + t_3\, e^{ik_x a}, \quad \text{(A3a)}$$

$$\langle 0|H_{\rm hop}|2\rangle = t_4(1 + e^{-ik_y b}), \quad \text{(A3b)}$$

$$\langle 0|H_{\rm hop}|3\rangle = t_2(1 + e^{-ik_x a}), \quad \text{(A3c)}$$

$$\langle 1|H_{\rm hop}|2\rangle = t_2\, e^{-ik_y b}(1 + e^{-ik_x a}), \quad \text{(A3d)}$$

$$\langle 1|H_{\rm hop}|3\rangle = t_4\, e^{-ik_x a}(1 + e^{-ik_y b}), \quad \text{(A3e)}$$

$$\langle 2|H_{\rm hop}|3\rangle = t_1 + t_3\, e^{-ik_x a}. \quad \text{(A3f)}$$

Here, diagonal entries $\langle i|H_{\rm hop}|i\rangle$ are zero for all i.

[1] N. Toyota, M. Lang, and J. Müller, *Low-Dimensional Molecular Metals* (Springer-Verlag, Berlin, 2007).

[2] B. J. Powell and R. H. McKenzie, Strong electronic correlations in superconducting organic charge transfer salts, J. Phys.: Condens. Matter **18**, R827 (2006).

[3] H. Elsinger, J. Wosnitza, S. Wanka, J. Hagel, D. Schweitzer, and W. Strunz, κ-(BEDT-TTF)$_2$Cu[N(CN)$_2$]Br: A Fully Gapped Strong-Coupling Superconductor, Phys. Rev. Lett. **84**, 6098 (2000).

[4] Y. Shimizu, K. Miyagawa, K. Kanoda, M. Maesato, and G. Saito, Spin Liquid State in an Organic Mott Insulator with a Triangular Lattice, Phys. Rev. Lett. **91**, 107001 (2003).

[5] Y. Kurosaki, Y. Shimizu, K. Miyagawa, K. Kanoda, and G. Saito, Mott Transition from a Spin Liquid to a Fermi Liquid in the Spin-Frustrated Organic Conductor κ-$(ET)_2Cu_2(CN)_3$, Phys. Rev. Lett. **95**, 177001 (2005).

[6] F. Kagawa, K. Miyagawa, and K. Kanoda, Unconventional critical behavior in a quasi-two-dimensional organic conductor, Nature (London) **436**, 534 (2005).

[7] R. H. McKenzie, Similarities between organic and cuprate superconductors, Science **278**, 820 (1997).

[8] J. Müller, M. Lang, R. Helfrich, R. Steglich, and T. Sasaki, High-resolution ac-calorimetry studies of the quasi-two-dimensional organic superconductor κ-(BEDT-TTF)$_2$Cu(NCS)$_2$, Phys. Rev. B **65**, 140509(R) (2002).

[9] J. Wosnitza, S. Wanka, J. Hagel, M. Reibelt, D. Schweitzer, and J. A. Schlueter, Thermodynamic properties of quasi-two-dimensional organic superconductors, Synth. Meth. **133–134**, 201 (2003).

[10] O. J. Taylor, A. Carrington, and J. A. Schlueter, Specific-Heat Measurements of the Gap Structure of the Organic Superconductors κ-$(ET)_2$Cu[N(CN)$_2$]Br and κ-$(ET)_2$Cu(NCS)$_2$, Phys. Rev. Lett. **99**, 057001 (2007).

[11] O. J. Taylor, A. Carrington, and J. A. Schlueter, Superconductor-insulator phase separation induced by rapid cooling of κ-$(ET)_2$Cu[N(CN)$_2$]Br, Phys. Rev. B **77**, 060503(R) (2008).

[12] L. Malone, O. J. Taylor, J. A. Schlueter, and A. Carrington, Location of gap nodes in the organic superconductors κ-$(ET)_2$Cu(NCS)$_2$ and κ-$(ET)_2$Cu[N(CN)$_2$]Br determined by magnetocalorimetry, Phys. Rev. B **82**, 014522 (2010).

[13] S. Milbradt, A. A. Bardin, C. J. S. Truncik, W. A. Huttema, A. C. Jacko, P. L. Burn, S. C. Lo, B. J. Powell, and D. M. Broun, In-plane superfluid density and microwave conductivity of the organic superconductor κ-$(ET)_2$Cu[N(CN)$_2$]Br: Evidence for d-wave pairing and resilient quasiparticles, Phys. Rev. B **88**, 064501 (2013).

[14] K. Izawa, H. Yamaguchi, T. Sasaki, and Y. Matsuda, Superconducting Gap Structure of κ-(BEDT-TTF)$_2$Cu(NCS)$_2$ Probed by Thermal Conductivity Tensor, Phys. Rev. Lett. **88**, 027002 (2001).

[15] J. M. Schrama, E. Rzepniewski, R. S. Edwards, J. Singleton, A. Ardavan, M. Kurmoo, and P. Day, Millimeter-Wave Magneto-Optical Determination of the Anisotropy of the Superconducting Order Parameter in the Molecular Superconductor κ-(BEDT-TTF)$_2$Cu(NCS)$_2$, Phys. Rev. Lett. **83**, 3041 (1999).

[16] T. Arai, K. Ichimura, K. Nomura, S. Takasaki, J. Yamada, S. Nakatsuji, and H. Anzai, Tunneling spectroscopy on the organic superconductor κ-(BEDT-TTF)$_2$Cu(NCS)$_2$ using STM, Phys. Rev. B **63**, 104518 (2001).

[17] K. Ichimura, M. Takami, and K. Nomura, Direct observation of d-wave superconducting gap in κ-(ET)$_2$Cu[N(CN)$_2$]Br with scanning tunneling microscopy, J. Phys. Soc. Jpn. **77**, 114707 (2008).

[18] Y. Oka, H. Nobukane, N. Matsunaga, K. Nomura, K. Katono, K. Ichimura, and A. Kawamoto, Tunneling spectroscopy in organic superconductor κ-(BEDT-TTF-d[3, 3])$_2$Cu[N(CN)$_2$]Br, J. Phys. Soc. Jpn. **84**, 064713 (2015).

[19] D. Guterding, S. Diehl, M. Altmeyer, T. Methfessel, U. Tutsch, H. Schubert, M. Lang, J. Müller, M. Huth, H. O. Jeschke, R. Valentí, M. Jourdan, and H.-J. Elmers, Evidence for Eight Node Mixed-Symmetry Superconductivity in a Correlated Organic Metal, Phys. Rev. Lett. **116**, 237001 (2016).

[20] M. Dion, D. Fournier, M. Poirier, K. D. Truong, and A.-M. S. Tremblay, Mixed pairing symmetry in κ-(BEDT-TTF)$_2$X organic superconductors from ultrasonic velocity measurements, Phys. Rev. B **80**, 220511(R) (2009).

[21] M. Tamura, H. Tajima, K. Yakushi, H. Kuroda, A. Kobayashi, R. Kato, and H. Kobayashi, Reflectance spectra of κ-(BEDT-TTF)$_2$I$_3$: Electronic structure of dimeric BEDT-TTF salts, J. Phys. Soc. Jpn. **60**, 3861 (1991).

[22] H. Kino and H. Fukuyama, Phase diagram of two-dimensional organic conductors: (BEDT-TTF)$_2$X, J. Phys. Soc. Jpn. **65**, 2158 (1996).

[23] K. Nakamura, Y. Yoshimoto, T. Kosugi, R. Arita, and M. Imada, Ab initio derivation of low-energy model for κ-ET type organic conductors, J. Phys. Soc. Jpn. **78**, 083710 (2009).

[24] H. C. Kandpal, I. Opahle. Y.-Z. Zhang, H. O. Jeschke, and R. Valentí, Revision of Model Parameters for κ-Type Charge Transfer Salts: An Ab Initio Study, Phys. Rev. Lett. **103**, 067004 (2009).

[25] H. O. Jeschke, M. de Souza, R. Valentí, R. S. Manna, M. Lang, and J. A. Schlueter, Temperature dependence of structural and electronic properties of the spin-liquid candidate kappa-(BEDT-TTF)$_2$Cu$_2$(CN)$_3$, Phys. Rev. B **85**, 035125 (2012).

[26] J. Schmalian, Pairing due to Spin Fluctuations in Layered Organic Superconductors, Phys. Rev. Lett. **81**, 4232 (1998).

[27] H. Kino and H. Kontani, Phase diagram of superconductivity on the anisotropic triangular lattice Hubbard model: An effective model of κ-(BEDT-TTF) salts, J. Phys. Soc. Jpn. **67**, 3691 (1998).

[28] H. Kondo and T. Moriya, Spin fluctuation-induced superconductivity in organic compounds, J. Phys. Soc. Jpn. **67**, 3695 (1998).

[29] A. Benali, Layered organic conductors κ-(BEDT-TTF)$_2$X: magnetic and superconducting properties, Synth. Meth. **175**, 120 (2013).

[30] H. Morita, S. Watanabe, and M. Imada, Nomagnetic Insulating states near the Mott transitions on lattices with geometrical frustration and implications for κ-(ET)$_2$Cu$_2$(CN)$_3$, J. Phys. Soc. Jpn. **71**, 2109 (2002).

[31] O. Parcollet, G. Biroli, and G. Kotliar, Cluster Dynamical Mean Field Analysis of the Mott Transition, Phys. Rev. Lett. **92**, 226402 (2004).

[32] B. Kyung and A.-M. S. Tremblay, Mott Transition, Antiferromagnetism, and d-Wave Superconductivity in Two-Dimensional Organic Conductors, Phys. Rev. Lett. **97**, 046402 (2006).

[33] C.-D. Hébert, P. Sémon, and A.-M. S. Tremblay, Superconducting dome in doped quasi-two-dimensional organic Mott insulators: A paradigm for strongly correlated superconductivity, Phys. Rev. B **92**, 195112 (2015).

[34] J. Liu, J. Schmalian, and N. Trivedi, Pairing and Superconductivity Driven by Strong Quasiparticle Renormalization in Two-Dimensional Organic Charge Transfer Salts, Phys. Rev. Lett. **94**, 127003 (2005).

[35] T. Watanabe, H. Yokoyama, Y. Tanaka, and J. Inoue, Superconductivity and a Mott transition in a Hubbard model on an anisotropic triangular lattice, J. Phys. Soc. Jpn. **75**, 074707 (2006).

[36] L. F. Tocchio, H. Feldner, F. Becca, R. Valentí, and C. Gros, Spin-liquid versus spiral-order phases in the anisotropic triangular lattice, Phys. Rev. B **87**, 035143 (2013).

[37] L. F. Tocchio, C. Gros, R. Valentí, and F. Becca, One-dimensional spin liquid, collinear, and spiral phases from uncoupled chains to the triangular lattice, Phys. Rev. B **89**, 235107 (2014).

[38] T. Koretsune, Y. Motome, and A. Furusaki, Exact diagonalization study of Mott transition in the Hubbard model on an anisotropic triangular lattice, J. Phys. Soc. Jpn. **76**, 074719 (2007).

[39] R. T. Clay, H. Li, and S. Mazumdar, Absence of Superconductivity in the Half-Filled Band Hubbard Model on the Anisotropic Triangular Lattice, Phys. Rev. Lett. **101**, 166403 (2008).

[40] D. J. Scalapino, A common thread: The pairing interaction for unconventional superconductors, Rev. Mod. Phys. **84**, 1383 (2012).

[41] S. Lefebvre, P. Wzietek, S. Brown, C. Bourbonnais, D. Jérome, C. Mézière, M. Formigué, and P. Batail, Mott Transition, Antiferromagnetism, and Unconventional Superconductivity in Layered Organic Superconductors, Phys. Rev. Lett. **85**, 5420 (2000).

[42] K. Miyagawa, K. Kanoda, and A. Kawamoto, NMR studies on two-dimensional molecular conductors and superconductors: Mott transition in κ-(BEDT-TTF)$_2X$, Chem. Rev. **104**, 5635 (2004).

[43] D. Guterding, R. Valentí, and H. O. Jeschke, Influence of molecular conformations on the electronic structure of organic charge transfer salts, Phys. Rev. B **92**, 081109(R) (2015).

[44] P. Lunkenheimer, J. Müller, S. Krohns, F. Schrettle, A. Loidl, B. Hartmann, R. Rommel, M. de Souza, C. Hotta, J. A. Schlueter, and M. Lang, Multiferroicity in an organic charge-transfer salt that is suggestive of electric-dipole-driven magnetism, Nat. Mater. **11**, 755 (2012).

[45] K. Kuroki, Pairing symmetry competition in organic superconductors, J. Phys. Soc. Jpn. **75**, 051013 (2006).

[46] A. Ardavan, S. Brown, S. Kagoshima, K. Kanoda, K. Kuroki, H. Mori, M. Ogata, S. Uji, and J. Wosnitza, Recent topics of organic superconductors, J. Phys. Soc. Jpn. **81**, 011004 (2012).

[47] K. Kuroki, T. Kimura, R. Arita, Y. Tanaka, and Y. Matsuda, $d_{x^2-y^2}$- versus d_{xy}-like pairings in organic superconductors κ-(BEDT-TTF)$_2$X, Phys. Rev. B **65**, 100516(R) (2002).

[48] H. Gomi, T. Imai, A. Takahashi, and M. Aihara, Purely electronic terahertz polarization in dimer Mott insulators, Phys. Rev. B **82**, 035101 (2010).

[49] C. Hotta, Quantum electric dipoles in spin-liquid dimer Mott insulator κ-ET$_2$Cu$_2$(CN)$_3$, Phys. Rev. B **82**, 241104(R) (2010).

[50] H. Shinaoka, T. Misawa, K. Nakamura, and M. Imada, Mott transition and phase diagram of κ-(BEDT-TTF)$_2$Cu(NCS)$_2$ studied by two-dimensional model derived from ab initio method, J. Phys. Soc. Jpn. **81**, 034701 (2012).

[51] T. Koretsune and C. Hotta, Evaluating model parameters of the κ- and β'-type Mott insulating organic solids, Phys. Rev. B **89**, 045102 (2014).

[52] K. Koepernik and H. Eschrig, Full-potential nonorthogonal local-orbital minimum-basis band-structure scheme, Phys. Rev. B **59**, 1743 (1999); http://www.FPLO.de.

[53] J. P. Perdew, K. Burke, and M. Ernzerhof, Generalized Gradient Approximation Made Simple, Phys. Rev. Lett. **77**, 3865 (1996).

[54] J. A. Schlueter, L. Wiehl, H. Park, M. de Souza, M. Lang, H.-J. Koo, and M.-H. Whangbo, Enhanced critical temperature in a dual-layered molecular superconductor, J. Am. Chem. Soc. **132**, 16308 (2010).

[55] T. Kawamoto, T. Mori, A. Nakao, Y. Murakami, and J. A. Schlueter, T_c of 11 K identified for the third polymorph of the (BEDT-TTF)$_2$Ag(CF$_3$)$_4$(TCE) organic superconductor, J. Phys. Soc. Jpn. **81**, 023705 (2012).

[56] T. Hiramatsu, Y. Yoshida, G. Saito, A. Otsuka, H. Yamochi, M. Maesato, Y. Shimizu, H. Ito, and H. Kishida, Quantum spin liquid: Design of a quantum spin liquid next to a superconducting state based on a dimer-type ET Mott insulator, J. Mater. Chem. C **3**, 1378 (2015).

[57] H. Eschrig and K. Koepernik, Tight-binding models for the iron-based superconductors, Phys. Rev. B **80**, 104503 (2009).

[58] B. S. Shastry and B. Sutherland, Exact ground state of a quantum mechanical antiferromagnet, Physica B **108**, 1069 (1981).

[59] M. Altmeyer, R. Valentí, and H. O. Jeschke, Role of layer packing for the electronic properties of the organic superconductor (BEDT-TTF)$_2$Ag(CF$_3$)$_4$(TCE), Phys. Rev. B **91**, 245137 (2015).

[60] E. Yusuf, B. J. Powell, and R. H. McKenzie, Antiferromagnetic spin fluctuations in the metallic phase of quasi-two-dimensional organic superconductors, Phys. Rev. B **75**, 214515 (2007).

[61] S. Graser, T. A. Maier, P. J. Hirschfeld, and D. J. Scalapino, Near-degeneracy of several pairing channels in multiorbital models for the Fe pnictides, New J. Phys. **11**, 025016 (2009).

[62] A. Kreisel, Y. Wang, T. A. Maier, P. J. Hirschfeld, and D. J. Scalapino, Spin-fluctuations and superconductivity in K$_x$Fe$_{2-y}$Se$_2$, Phys. Rev. B **88**, 094522 (2013).

[63] D. Guterding, H. O. Jeschke, P. J. Hirschfeld, and R. Valentí, Unified picture of the doping dependence of superconducting transition temperatures in alkali metal/ammonia intercalated FeSe, Phys. Rev. B **91**, 041112(R) (2015).

[64] D. Guterding, S. Backes, H. O. Jeschke, and R. Valentí, Origin of the superconducting state in the collapsed tetragonal phase of KFe$_2$As$_2$, Phys. Rev. B **91**, 140503(R) (2015).

[65] N. E. Bickers, D. J. Scalapino, and S. R. White, Conserving Approximations for Strongly Correlated Electron Systems: Bethe-Salpeter Equation and Dynamics for the Two-Dimensional Hubbard Model, Phys. Rev. Lett. **62**, 961 (1989).

[66] D. J. Scalapino, E. Loh, Jr., and J. E. Hirsch, d-wave pairing near a spin-density-wave instability, Phys. Rev. B **34**, 8190 (1986).

[67] J. Bardeen, L. N. Cooper, and J. R. Schrieffer, Theory of superconductivity, Phys. Rev. **108**, 1175 (1957).

[68] Y. Tanaka and S. Kashiwaya, Theory of Tunneling Spectroscopy of d-Wave Superconductors, Phys. Rev. Lett. **74**, 3451 (1995).

[69] Y. Hasegawa, Density of states and NMR relaxation rate in anisotropic superconductivity with intersecting line nodes, J. Phys. Soc. Jpn. **65**, 3131 (1996).

[70] R. C. Dynes, V. Narayanamurti, and J. P. Garno, Direct Measurement of Quasiparticle-Lifetime Broadening in a Strong-Coupled Superconductor, Phys. Rev. Lett. **41**, 1509 (1978).

[71] S. Diehl, T. Methfessel, U. Tutsch, J. Müller, M. Lang, M. Huth, M. Jourdan, and H.-J. Elmers, Disorder-induced gap in the normal density of states of the organic superconductor κ-(BEDT-TTF)$_2$Cu[N(CN)$_2$]Br, J. Phys.: Condens. Matter **27**, 265601 (2015).

[72] R. Kato, H. Kobayashi, A. Kobayashi, S. Moriyama, Y. Nishio, K. Kajita, and W. Sasaki, A new ambient-pressure superconductor, κ-(BEDT-TTF)$_2$I$_3$, Chem. Lett. **16**, 507 (1987).

[73] H. Mori, I. Hirabayashi, S. Tanaka, T. Mori, and H. Inokuchi, A new ambient-pressure superconductor, κ-(BEDT-TTF)$_2$Ag(CN)$_2$H$_2$O ($T_c = 5.0$ K), Solid State Commun. **76**, 35 (1990).

[74] A. M. Kini, U. Geiser, H. H. Wang, K. D. Carlson, J. M. Williams, W. K. Kwok, K. G. Vandervoort, J. E. Thompson, D. L. Stupka, D. Jung, and M.-H. Whangbo, A new ambient-pressure organic superconductor, κ-(ET)$_2$Cu[N(CN)$_2$]Br, with the highest transition temperature yet observed (inductive onset $T_c = 11.6$ K, resistive onset = 12.5 K), Inorg. Chem. **29**, 2555 (1990).

[75] A. T. Rømer, A. Kreisel, I. Eremin, M. A. Malakhov, T. A. Maier, P. J. Hirschfeld, and B. M. Andersen, Pairing symmetry of the one-band Hubbard model in the paramagnetic weak-coupling limit: A numerical RPA study, Phys. Rev. B **92**, 104505 (2015).

[76] H. Hosono and K. Kuroki, Iron-based superconductors: Current status of materials and pairing mechanism, Physica C **514**, 399 (2015).

[77] J. G. Analytis, A. Ardavan, S. J. Blundell, R. L. Owen, E. F. Garman, C. Jeynes, and B. J. Powell, Effect of Irradiation-Induced Disorder on the Conductivity and Critical Temperature of the Organic Superconductor κ-(BEDT-TTF)$_2$Cu(SCN)$_2$, Phys. Rev. Lett. **96**, 177002 (2006).

[78] K. Sano, T. Sasaki, N. Yoneyama, and N. Kobayashi, Electron Localization Near the Mott Transition in the Organic Superconductor κ-(BEDT-TTF)$_2$Cu[N(CN)$_2$]Br, Phys. Rev. Lett. **104**, 217003 (2010).

[79] B. Hartmann, J. Müller, and T. Sasaki, Mott metal-insulator transition induced by utilizing a glasslike structural ordering in low-dimensional molecular conductors, Phys. Rev. B **90**, 195150 (2014).

[80] J. Müller, B. Hartmann, R. Rommel, J. Brandenburg, S. M. Winter, and J. A. Schlueter, Origin of the glass-like dynamics in molecular metals κ-(BEDT-TTF)$_2$X: Implications from fluctuation spectroscopy and ab initio calculations, New J. Phys. **17**, 083057 (2015).